Transverse-single-spin asymmetries of charged pions at midrapidity in transversely polarized $p + p$ collisions at $\sqrt{s} = 200$ GeV

U. A. Acharya,[20] C. Aidala,[40] Y. Akiba,[53,54,*] M. Alfred,[22] V. Andrieux,[40] N. Apadula,[27] H. Asano,[33,53] B. Azmoun,[7] V. Babintsev,[23] N. S. Bandara,[39] K. N. Barish,[8] S. Bathe,[5,54] A. Bazilevsky,[7] M. Beaumier,[8] R. Belmont,[11,46] A. Berdnikov,[56] Y. Berdnikov,[56] L. Bichon,[64] B. Blankenship,[64] D. S. Blau,[32,43] J. S. Bok,[45] V. Borisov,[56] M. L. Brooks,[35] J. Bryslawskyj,[5,8] V. Bumazhnov,[23] S. Campbell,[12] V. Canoa Roman,[59] R. Cervantes,[59] M. Chiu,[7] C. Y. Chi,[12] I. J. Choi,[24] J. B. Choi,[29,†] Z. Citron,[65] M. Connors,[20,54] R. Corliss,[59] N. Cronin,[59] T. Csörgő,[16,66] M. Csanád,[15] T. W. Danley,[47] M. S. Daugherity,[1] G. David,[7,59] K. DeBlasio,[44] K. Dehmelt,[59] A. Denisov,[23] A. Deshpande,[54,59] E. J. Desmond,[7] A. Dion,[59] D. Dixit,[59] J. H. Do,[67] A. Drees,[59] K. A. Drees,[6] J. M. Durham,[35] A. Durum,[23] H. En'yo,[53] A. Enokizono,[53,55] R. Esha,[59] S. Esumi,[63] B. Fadem,[41] W. Fan,[59] N. Feege,[59] D. E. Fields,[44] M. Finger, Jr.,[9] M. Finger,[9] D. Fitzgerald,[40] S. L. Fokin,[32] J. E. Frantz,[47] A. Franz,[7] A. D. Frawley,[19] Y. Fukuda,[63] P. Gallus,[13] C. Gal,[59] P. Garg,[3,59] H. Ge,[59] M. Giles,[59] F. Giordano,[24] Y. Goto,[53,54] N. Grau,[2] S. V. Greene,[64] M. Grosse Perdekamp,[24] T. Gunji,[10] H. Guragain,[20] T. Hachiya,[42,53,54] J. S. Haggerty,[7] K. I. Hahn,[17] H. Hamagaki,[10] H. F. Hamilton,[1] J. Hanks,[59] S. Y. Han,[17,31] M. Harvey,[61] S. Hasegawa,[28] T. O. S. Haseler,[20] T. K. Hemmick,[59] X. He,[20] J. C. Hill,[27] K. Hill,[11] A. Hodges,[20] R. S. Hollis,[8] K. Homma,[21] B. Hong,[31] T. Hoshino,[21] N. Hotvedt,[27] J. Huang,[7] K. Imai,[28] M. Inaba,[63] A. Iordanova,[8] D. Isenhower,[1] D. Ivanishchev,[51] B. V. Jacak,[59] M. Jezghani,[20] X. Jiang,[35] Z. Ji,[59] B. M. Johnson ⦿,[7,20] D. Jouan,[49] D. S. Jumper,[24] J. H. Kang,[67] D. Kapukchyan,[8] S. Karthas,[59] D. Kawall,[39] A. V. Kazantsev,[32] V. Khachatryan,[59] A. Khanzadeev,[51] A. Khatiwada,[35] C. Kim,[8,31] E.-J. Kim,[29] M. Kim,[57] T. Kim,[17] D. Kincses,[15] A. Kingan,[59] E. Kistenev,[7] J. Klatsky,[19] P. Kline,[59] T. Koblesky,[11] D. Kotov,[51,56] L. Kovacs,[15] S. Kudo,[63] K. Kurita,[55] Y. Kwon,[67] J. G. Lajoie,[27] D. Larionova,[56] A. Lebedev,[27] S. Lee,[67] S. H. Lee,[27,40,59] M. J. Leitch,[35] Y. H. Leung,[59] N. A. Lewis,[40] S. H. Lim,[35,52,67] M. X. Liu,[35] X. Li,[35] V.-R. Loggins,[24] D. A. Loomis,[40] K. Lovasz,[14] D. Lynch,[7] S. Lökös,[15] T. Majoros,[14] Y. I. Makdisi,[6] M. Makek,[68] V. I. Manko,[32] E. Mannel,[7] M. McCumber,[35] P. L. McGaughey,[35] D. McGlinchey,[11,35] C. McKinney,[24] M. Mendoza,[8] A. C. Mignerey,[38] A. Milov,[65] D. K. Mishra,[4] J. T. Mitchell,[7] M. Mitrankova,[56] Iu. Mitrankov,[56] Iu. Mitrankov,[56] G. Mitsuka,[30,54] S. Miyasaka,[53,62] S. Mizuno,[53,63] M. M. Mondal,[59] P. Montuenga,[24] T. Moon,[31,67] D. P. Morrison,[7] B. Mulilo,[31,53] T. Murakami,[33,53] J. Murata,[53,55] K. Nagai,[62] K. Nagashima,[21] T. Nagashima,[55] J. L. Nagle,[11] M. I. Nagy,[15] I. Nakagawa,[53,54] K. Nakano,[53,62] C. Nattrass,[60] S. Nelson,[18] T. Niida,[63] R. Nouicer,[7,54] T. Novák,[16,66] N. Novitzky,[59,63] G. Nukazuka,[53,54] A. S. Nyanin,[32] E. O'Brien,[7] C. A. Ogilvie,[27] J. D. Orjuela Koop,[11] J. D. Osborn,[40,48] A. Oskarsson,[36] G. J. Ottino,[44] K. Ozawa,[30,63] V. Pantuev,[25] V. Papavassiliou,[45] J. S. Park,[57] S. Park,[53,57,59] M. Patel,[27] S. F. Pate,[45] W. Peng,[64] D. V. Perepelitsa,[7,11] G. D. N. Perera,[45] D. Yu. Peressounko,[32] C. E. PerezLara,[59] J. Perry,[27] R. Petti,[7] M. Phipps,[7,24] C. Pinkenburg,[7] R. P. Pisani,[7] M. Potekhin,[7] A. Pun,[47] M. L. Purschke,[7] P. V. Radzevich,[56] N. Ramasubramanian,[59] K. F. Read,[48,60] D. Reynolds,[58] V. Riabov,[43,51] Y. Riabov,[51,56] D. Richford,[5] T. Rinn,[24,27] S. D. Rolnick,[8] M. Rosati,[27] Z. Rowan,[5] J. Runchey,[27] A. S. Safonov,[56] T. Sakaguchi,[7] H. Sako,[28] V. Samsonov,[43,51] M. Sarsour,[20] S. Sato,[28] B. Schaefer,[64] B. K. Schmoll,[60] K. Sedgwick,[8] R. Seidl,[53,54] A. Sen,[27,60] R. Seto,[8] A. Sexton,[38] D. Sharma,[59] I. Shein,[23] T.-A. Shibata,[53,62] K. Shigaki,[21] M. Shimomura,[27,42] T. Shioya,[63] P. Shukla,[4] A. Sickles,[24] C. L. Silva,[35] D. Silvermyr,[36] B. K. Singh,[3] C. P. Singh,[3] V. Singh,[3] M. Slunečka,[9] K. L. Smith,[19] M. Snowball,[35] R. A. Soltz,[34] W. E. Sondheim,[35] S. P. Sorensen,[60] I. V. Sourikova,[7] P. W. Stankus,[48] S. P. Stoll,[7] T. Sugitate,[21] A. Sukhanov,[7] T. Sumita,[53] J. Sun,[59] Z. Sun,[14] J. Sziklai,[66] K. Tanida,[28,54,57] M. J. Tannenbaum,[7] S. Tarafdar,[64,65] A. Taranenko,[43] G. Tarnai,[14] R. Tieulent,[20,37] A. Timilsina,[27] A. Timilsina,[27] T. Todoroki,[53,54,63] M. Tomášek,[13] C. L. Towell,[1] R. S. Towell,[1] I. Tserruya,[65] Y. Ueda,[21] B. Ujvari,[14] H. W. van Hecke,[35] J. Velkovska,[64] M. Virius,[13] V. Vrba,[13,26] N. Vukman,[68] X. R. Wang,[45,54] Y. S. Watanabe,[10] C. P. Wong,[20,35] C. L. Woody,[7] L. Xue,[20] C. Xu,[45] Q. Xu,[64] S. Yalcin,[59] Y. L. Yamaguchi,[59] H. Yamamoto,[63] A. Yanovich,[23] I. Yoon,[57] J. H. Yoo,[31] I. E. Yushmanov,[32] H. Yu,[45,50] W. A. Zajc,[12] A. Zelenski,[6] S. Zharko,[56] and L. Zou[8]

(PHENIX Collaboration)

[1]*Abilene Christian University, Abilene, Texas 79699, USA*
[2]*Department of Physics, Augustana University, Sioux Falls, South Dakota 57197, USA*
[3]*Department of Physics, Banaras Hindu University, Varanasi 221005, India*
[4]*Bhabha Atomic Research Centre, Bombay 400 085, India*
[5]*Baruch College, City University of New York, New York, New York, 10010 USA*
[6]*Collider-Accelerator Department, Brookhaven National Laboratory, Upton, New York 11973-5000, USA*
[7]*Physics Department, Brookhaven National Laboratory, Upton, New York 11973-5000, USA*
[8]*University of California-Riverside, Riverside, California 92521, USA*
[9]*Charles University, Ovocný trh 5, Praha 1, 116 36, Prague, Czech Republic*

[10]*Center for Nuclear Study, Graduate School of Science, University of Tokyo,*
7-3-1 Hongo, Bunkyo, Tokyo 113-0033, Japan
[11]*University of Colorado, Boulder, Colorado 80309, USA*
[12]*Columbia University, New York, New York 10027 and Nevis Laboratories,*
Irvington, New York 10533, USA
[13]*Czech Technical University, Zikova 4, 166 36 Prague 6, Czech Republic*
[14]*Debrecen University, H-4010 Debrecen, Egyetem tér 1, Hungary*
[15]*ELTE, Eötvös Loránd University, H-1117 Budapest, Pázmány P. s. 1/A, Hungary*
[16]*Eszterházy Károly University, Károly Róbert Campus, H-3200 Gyöngyös, Mátrai út 36, Hungary*
[17]*Ewha Womans University, Seoul 120-750, Korea*
[18]*Florida A&M University, Tallahassee, Florida 32307, USA*
[19]*Florida State University, Tallahassee, Florida 32306, USA*
[20]*Georgia State University, Atlanta, Georgia 30303, USA*
[21]*Hiroshima University, Kagamiyama, Higashi-Hiroshima 739-8526, Japan*
[22]*Department of Physics and Astronomy, Howard University, Washington, D.C. 20059, USA*
[23]*IHEP Protvino, State Research Center of Russian Federation, Institute for High Energy Physics,*
Protvino 142281, Russia
[24]*University of Illinois at Urbana-Champaign, Urbana, Illinois 61801, USA*
[25]*Institute for Nuclear Research of the Russian Academy of Sciences,*
prospekt 60-letiya Oktyabrya 7a, Moscow 117312, Russia
[26]*Institute of Physics, Academy of Sciences of the Czech Republic,*
Na Slovance 2, 182 21 Prague 8, Czech Republic
[27]*Iowa State University, Ames, Iowa 50011, USA*
[28]*Advanced Science Research Center, Japan Atomic Energy Agency,*
2-4 Shirakata Shirane, Tokai-mura, Naka-gun, Ibaraki-ken 319-1195, Japan
[29]*Jeonbuk National University, Jeonju 54896, Korea*
[30]*KEK, High Energy Accelerator Research Organization, Tsukuba, Ibaraki 305-0801, Japan*
[31]*Korea University, Seoul 02841, Korea*
[32]*National Research Center "Kurchatov Institute,"Moscow, 123098 Russia*
[33]*Kyoto University, Kyoto 606-8502, Japan*
[34]*Lawrence Livermore National Laboratory, Livermore, California 94550, USA*
[35]*Los Alamos National Laboratory, Los Alamos, New Mexico 87545, USA*
[36]*Department of Physics, Lund University, Box 118, SE-221 00 Lund, Sweden*
[37]*IPNL, CNRS/IN2P3, Univ Lyon, Université Lyon 1, F-69622, Villeurbanne, France*
[38]*University of Maryland, College Park, Maryland 20742, USA*
[39]*Department of Physics, University of Massachusetts, Amherst, Massachusetts 01003-9337, USA*
[40]*Department of Physics, University of Michigan, Ann Arbor, Michigan 48109-1040, USA*
[41]*Muhlenberg College, Allentown, Pennsylvania 18104-5586, USA*
[42]*Nara Women's University, Kita-uoya Nishi-machi Nara 630-8506, Japan*
[43]*National Research Nuclear University, MEPhI, Moscow Engineering Physics Institute,*
Moscow, 115409, Russia
[44]*University of New Mexico, Albuquerque, New Mexico 87131, USA*
[45]*New Mexico State University, Las Cruces, New Mexico 88003, USA*
[46]*Physics and Astronomy Department, University of North Carolina at Greensboro,*
Greensboro, North Carolina 27412, USA
[47]*Department of Physics and Astronomy, Ohio University, Athens, Ohio 45701, USA*
[48]*Oak Ridge National Laboratory, Oak Ridge, Tennessee 37831, USA*
[49]*IPN-Orsay, Univ. Paris-Sud, CNRS/IN2P3, Université Paris-Saclay, BP1, F-91406 Orsay, France*
[50]*Peking University, Beijing 100871, People's Republic of China*
[51]*PNPI, Petersburg Nuclear Physics Institute, Gatchina, Leningrad region, 188300, Russia*
[52]*Pusan National University, Pusan 46241, Korea*
[53]*RIKEN Nishina Center for Accelerator-Based Science, Wako, Saitama 351-0198, Japan*
[54]*RIKEN BNL Research Center, Brookhaven National Laboratory, Upton, New York 11973-5000, USA*
[55]*Physics Department, Rikkyo University, 3-34-1 Nishi-Ikebukuro, Toshima, Tokyo 171-8501, Japan*
[56]*Saint Petersburg State Polytechnic University, St. Petersburg 195251, Russia*
[57]*Department of Physics and Astronomy, Seoul National University, Seoul 151-742, Korea*
[58]*Chemistry Department, Stony Brook University, SUNY, Stony Brook, New York 11794-3400, USA*
[59]*Department of Physics and Astronomy, Stony Brook University,*
SUNY, Stony Brook, New York 11794-3800, USA
[60]*University of Tennessee, Knoxville, Tennessee 37996, USA*

[61]*Texas Southern University, Houston, Texas 77004, USA*
[62]*Department of Physics, Tokyo Institute of Technology, Oh-okayama, Meguro, Tokyo 152-8551, Japan*
[63]*Tomonaga Center for the History of the Universe, University of Tsukuba, Tsukuba, Ibaraki 305, Japan*
[64]*Vanderbilt University, Nashville, Tennessee 37235, USA*
[65]*Weizmann Institute, Rehovot 76100, Israel*
[66]*Institute for Particle and Nuclear Physics, Wigner Research Centre for Physics, Hungarian Academy of Sciences (Wigner RCP, RMKI) H-1525 Budapest 114, POBox 49, Budapest, Hungary*
[67]*Yonsei University, IPAP, Seoul 120-749, Korea*
[68]*Department of Physics, Faculty of Science, University of Zagreb, Bijenička c. 32 HR-10002 Zagreb, Croatia*

In 2015, the PHENIX Collaboration has measured single-spin asymmetries for charged pions in transversely polarized $p + p$ collisions at the center-of-mass energy of $\sqrt{s} = 200$ GeV. The pions were detected at central rapidities of $|\eta| < 0.35$. The single-spin asymmetries are consistent with zero for each charge individually, as well as consistent with the previously published neutral-pion asymmetries in the same rapidity range. However, they show a slight indication of charge-dependent differences which may suggest a flavor dependence in the underlying mechanisms that create these asymmetries.

I. INTRODUCTION

Single-spin asymmetries have been measured in hadronic collisions over a wide range of energies for a number of final state particles [1–4] and at various rapidity regions. Initially, calculations that were based entirely on perturbative quantum chromodynamics (pQCD) expected such asymmetries to be suppressed as they generally required a helicity flip which would be proportional to the parton mass over the hard scale of the scattering process [5], though recent calculations suggest that perturbative contributions may be possible [6]. In contrast to the pQCD calculations, the measured single-spin asymmetries, A_N for pion production in the forward direction, were found to be quite sizeable [1–3].

Initially, two different mechanisms were suggested to describe these asymmetries that attribute the effect to the nonperturbative parts of either the parton distribution functions [7] or the fragmentation functions [8]. To do so, the traditional concept of parton distribution and fragmentation functions had to be extended to allow for explicit-transverse-momentum degrees of freedom. In the transverse-momentum-dependent (TMD) framework, it is however necessary that at least two scales are observed, the large scattering scale and a smaller scale related to the

intrinsic transverse momenta of parton distribution and fragmentation. Both can be observed in semi-inclusive deeply inelastic scattering (SIDIS), as was first successfully demonstrated in [9] for both suggested effects.

Single-hadron final-state measurements in hadronic collisions have only one scale, typically given by the transverse momentum of the detected hadron. As such, a collinear framework that only relies on a single hard scale was suggested to describe these asymmetries [10,11]. In this framework, nonzero asymmetries require nonperturbative higher-twist correlations either in the initial state or the final state [12,13]. Subsequently, it was suggested that some of these correlation functions can be related to transverse-momentum moments of the TMD functions [14], which unifies both approaches. Thus, global fits of asymmetry measurements from SIDIS and hadron collisions have become possible and provide additional precision on the underlying functions of interest such as the quark transversity [15] or the Sivers [7] function in the proton. The latest of these comes from [16], in which are found sizeable contributions from both initial- and final-state effects. However, the final-state effects dominate in hadronic collisions where the measured asymmetries are large.

Pion transverse-single-spin asymmetries pick up both initial- and final-state effects. While at forward rapidities, the asymmetries are quite sizeable in the energy range of the Relativistic Heavy Ion Collider (RHIC) at Brookhaven National Laboratory [2,3], neutral-pion and η mesons have been shown to have vanishing asymmetries at central rapidities where the valence effects are expected to be less pronounced [17]. In addition, in neutral-particle asymmetries, potential cancellations between different parton flavors could also cause these asymmetries to vanish. Charged

pion asymmetries provide different flavor sensitivity via the fragmentation functions and could test whether such cancellations happen, as the dominant hard process at the transverse momenta of this measurement is given by quark-gluon scattering. The PHENIX detector at RHIC has measured charged pion single-spin asymmetries at central rapidities in transversely polarized $p + p$ collisions at a center-of-mass energy of $\sqrt{s} = 200$ GeV.

In the following sections, the relevant detector systems and the accumulated datasets will be described. The documentation of the charged pion selection criteria, reconstruction efficiencies and various background corrections follow before evaluating the various systematic uncertainties for the asymmetry results which are then discussed.

II. DATASETS

In 2015, the PHENIX experiment accumulated 60 pb^{-1} of transversely polarized $p + p$ collision data. As both beams were polarized with average polarizations of 60% (counterclockwise, yellow beam) and 58% (clockwise, blue beam) [18], two independent measurements were initially performed using the spin information of one beam and averaging over the spin information of the second beam. After confirming the consistency of the single-spin asymmetries for each individual beam, the results were combined.

The PHENIX detector comprises a central Helmholtz double coil magnet that is surrounded by two central detector arms that cover 90 degrees azimuthally each, and a pseudorapidity range of $|\eta| < 0.35$. A detailed detector description can be found at [19], while only the detector subsystems relevant for this analysis will be presented in this paper. The central arms comprise drift (DC) and pad chambers (PC) at radii of 2.02–2.46 m (DC), 2.50 m (PC1), 4.00 m (PC2), and 5.00 m (PC3) that measure charged-particle momenta via the bending in the magnetic field. Between them, the gas ring-imaging Čerenkov (RICH) detector is situated that helps identifying electrons, pions, and kaons at momentum thresholds of 0.03, 4.7, and 16 GeV/c, respectively. Downstream of the PCs, two types of electromagnetic calorimeters, EMCal, are located. Six of eight sectors are instrumented with a lead-scintillator (PbSc) shashlik calorimeter while the remaining two sectors are instrumented with a lead-glass (PbGl) calorimeter. The EMCal measures the energy of electrons and photons, as well as in part the energy of hadrons that start showering within the EMCal detector. The PbSc (PbGl) EMCal corresponds to 0.85 (1.05) nuclear interaction lengths. It also serves as a trigger detector for these particles, where typically three different energy thresholds are set up with different suppression factors in the data taking.

Additionally, the beam-beam counters (BBCs), which comprise 64 quartz crystals and photomultipliers each, located at the forward and backward rapidities of $3.1 < |\eta| < 3.9$ register hard collisions and the collision vertex position and the start time for time-of-flight measurements. The BBCs also serve to log the relative luminosities that have been accumulated in different spin states. Zero-degree calorimeters at rapidities of $|\eta| > 6$ are used to cross check these relative luminosities as well as the correct beam spin orientation using the nonzero neutron single-spin asymmetries [20].

III. EVENT AND PARTICLE SELECTION CRITERIA

Pion-candidate events were selected if the lowest threshold of the EMCal trigger condition was satisfied, which required that at least 1.4 GeV of energy was deposited by the candidate particle in any of 4×4 EMCal towers. The BBC reconstructed event vertex had to be within 30 cm of the nominal beam interaction point along the beam axis. Pions were then selected if their momentum was between 5 and 15 GeV/c and the track matched the energy deposit in the EMCal. The track had to fire the RICH, and the shower shape in the EMCal had not to resemble that of an electromagnetic particle as given by a likelihood ratio between electromagnetic and other particles. To reduce the contamination by electrons in the pion data sample, the ratio of deposited energy, E, in the EMCal and reconstructed momentum, p, had to be $0.2 < E/p < 0.8$. At low E/p values, electrons that are produced in decays close to the EMCal and appear to have higher reconstructed momenta get rejected. While other electrons deposit all of their energy in the EMCal and typically get reconstructed at E/p values around unity, pions only deposit a fraction of their energy in the EMCal and can thus be selected.

To estimate the asymmetries for electron background an electron-enhanced sample is selected in addition to the pion-enhanced sample. For this sample the E/p and shower shape selections are inverted and even more RICH activity was required. These two types of samples will be denoted as pion-enhanced and electron-enhanced samples.

IV. ASYMMETRY EXTRACTION

The charged-pion yields were extracted starting by selecting them with the aforementioned criteria.

The single-spin asymmetries are then calculated for each beam, particle charge and signal type as

$$A_N = \frac{1}{P} \frac{\sqrt{N_L^\uparrow N_R^\downarrow} - \sqrt{N_L^\downarrow N_R^\uparrow}}{\sqrt{N_L^\uparrow N_R^\downarrow} + \sqrt{N_L^\downarrow N_R^\uparrow}}, \qquad (1)$$

where $N_{L/R}^{\uparrow/\downarrow}$ are the count rates to the left and right with respect to the polarized beam direction and spin orientation, for beams polarized up or down, respectively. P is the

average beam polarization. Additionally, as the detector sits not exactly at 90 degrees to the spin orientation, the asymmetry needs to be normalized with the average cosine of the azimuthal angle $\langle |\cos \phi| \rangle$ of all particle candidates n, $\langle |\cos \phi| \rangle = \sum_i |\cos \phi_i|/n$, where ϕ_i is defined for each candidate i relative to the spin orientation of the polarized beam, along its beam axis.

To evaluate the signal and background fractions in each sample, the raw candidate yields were corrected for the general reconstruction and acceptance efficiencies that were evaluated in single-particle simulations in GEANT3 [21]. The trigger efficiencies were corrected by calculating the fraction of minimum-bias events, for which pion candidates were also triggered by the EMCal based trigger. The RICH efficiency was calculated similarly by comparing the ratio of pion candidates that require the RICH selection criterion over all candidates. Because electrons also fulfill the RICH requirements for lower transverse momenta, the RICH efficiencies were corrected for this background using PYTHIA6 [22] simulations.

Given that pion candidates are triggered using an electromagnetic calorimeter, the overall reconstruction efficiencies are much lower than for neutral pions or electrons, see for example [23] for more details on pion cross section measurements using PHENIX.

The composition of the raw data yields as a function of the transverse momentum based on a PYTHIA6 [22] Monte-Carlo (MC) simulation is shown in Fig. 1, which shows that overall the data is well described by the MC. The thresholds in the RICH for pions and kaons to emit Čerenkov light are clearly visible at momenta of around 5 and 16 GeV/c, respectively. The simulations confirm that the selected sample is clearly dominated by pions, with electrons being the main background. To calibrate the actual signal and background fractions in the pion- and electron-enhanced
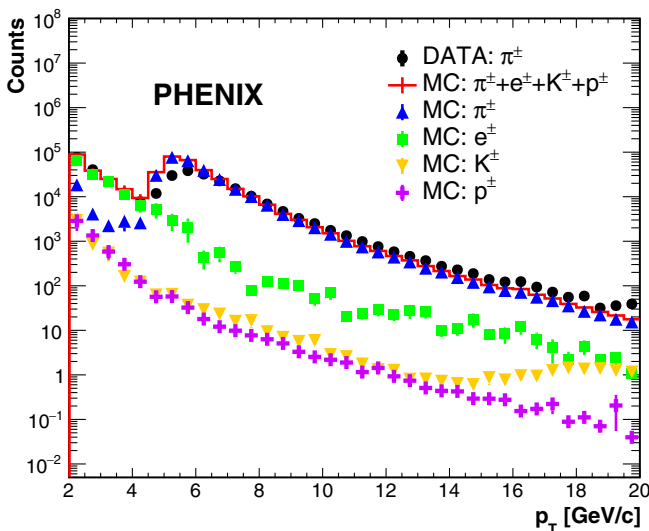
data samples, the E/p distributions in both pion- and electron-enhanced data samples were fit by the shapes obtained from MC over an enlarged E/p range. In particular, the electron contribution can be obtained by fitting a Gaussian close to unity which corresponds to the well-reconstructed electrons, that lose all their energy in the calorimeter, while the shape for the pions was directly taken from the simulation. The example for the raw yields and fits to the pion-enhanced data sample can be seen in Fig. 2. The MC obtains the overall magnitude of signal and background well, although slight differences between MC and data based electron peaks are visible that are used to rescale the background fraction. The background level in the pion-enhanced sample ranges from 1% to 8% for the different transverse-momentum bins and charges.

Using the extracted electron background fractions in pion-enhanced (r_π) and electron-enhanced (r_e) samples, as well as the sample's respective asymmetries (A_N^{Sig}, A_N^{BG}), the charged-pion asymmetries A_N^π can be obtained:

$$A_N^\pi = \frac{r_e A_N^{\text{Sig}} - r_\pi A_N^{\text{BG}}}{r_e - r_\pi}. \qquad (2)$$

The background asymmetries are consistent with zero, but their measured values were taken and the statistical errors propagated. The uncertainties on the signal to background fractions are assigned as systematic uncertainties as described below.

FIG. 1. Transverse-momentum distribution of reconstructed particles from data and MC simulation.
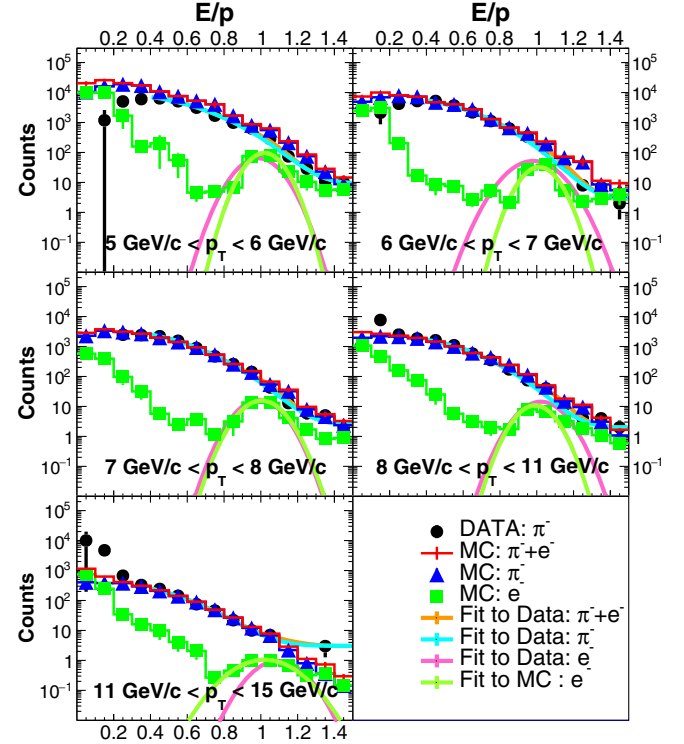

FIG. 2. Energy-over-momentum ratio distribution for negative pion and electron candidates from data and MC simulation for the pion-enhanced data sample.

V. SYSTEMATIC STUDIES AND CROSS CHECKS

For the asymmetries, several methods were applied to ensure the validity of the results. Apart from the previously discussed square root formula [Eq. (1)], the single-spin asymmetries were also extracted by the so-called relative luminosity formula, where the relative luminosity $\mathcal{R} = \mathcal{L}^{\uparrow}/\mathcal{L}^{\downarrow}$ between the luminosities of the two spin orientations is applied to the count rate differences and the count rate sum:

$$A_N = \frac{1}{P} \frac{N_L^{\uparrow} - \mathcal{R} N_L^{\downarrow}}{N_L^{\uparrow} + \mathcal{R} N_L^{\downarrow}}, \qquad (3)$$

and normalized by the acceptance factor $\langle |\cos \phi| \rangle$.

The asymmetries were additionally calculated as a function of the azimuthal angle and fitted with a sine modulation, although the azimuthal acceptance is limited at central rapidities in PHENIX. All three methods were compared using T tests and were found to be consistent with each other such that no further systematic uncertainty was assigned.

The two polarized beams provide two independent measurements of the asymmetries at central rapidities and can therefore be compared with each other for consistency. Again using a T test, the results were found to be consistent with each other, such that both results could be combined in the final result.

Another test is performed by randomizing the spin information of each of the beam crossings and fills to artificially remove any physical asymmetry. This so-called bunch-shuffling method is repeated many times and ideally should produce a Gaussian distribution centered at zero with a width as large as the statistical uncertainty. Any deviations would suggest additional systematic uncertainties that had not been included. While the bunch-shuffled asymmetries were on average consistent with zero, their widths were in some bins slightly larger than the statistical uncertainties. This variation was assigned as additional systematic uncertainty.

Lastly, the signal and background fractions that were described in the previous section were varied according to the uncertainties obtained from the fits to the E/p distribution. These are the dominant systematic uncertainty, but the measurements are dominated by the statistical uncertainties for both charges and all transverse-momentum bins. Additionally, a global 3.4% scale uncertainty exists due to the precision of the beam polarization evaluated by the RHIC polarimetry group [18].

VI. RESULTS

The asymmetries are displayed in Fig. 3 as a function of the transverse momentum and summarized in Table I. As can be seen, the results are statistically limited due to the fact that, in comparison to the neutral pions, only a fraction
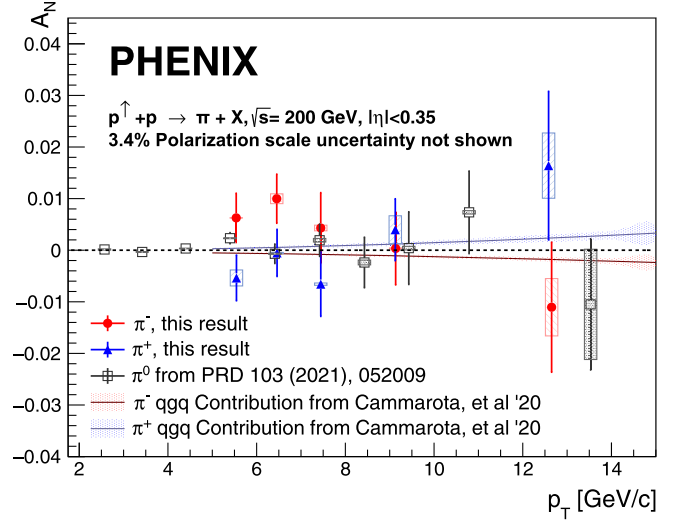

FIG. 3. Transverse-single-spin asymmetries as a function of transverse momentum for positive [closed (blue) triangles], negative [closed (red) circles], and the previously published neutral pions [open (black) boxes]. The statistical uncertainties are shown by bars and the systematic uncertainties are shown by boxes. The lower (red) and upper (blue) curves show the predicted A_N and their uncertainties based on Ref. [16].

of charged pions shower in the EMCal and fire triggers. Nevertheless, smaller than one percent level precision can be reached at lower transverse momenta, and the systematic uncertainties are generally much smaller. While the asymmetries for each charge are consistent with zero, as well as consistent with the previously measured neutral-pion asymmetries, there are differences between positive and negative charges. The χ^2 between π^+ and π^- asymmetries is 9.04 for all five data points together. This might indicate a dependence of the asymmetries on the participating flavors of up and down quarks in particular, given that gluon-related initial-state effects would show the same behavior

TABLE I. Final single-spin asymmetries for charged pions as a function of transverse momentum with statistical errors (ΔA_N) and systematic uncertainties (δA_N). An additional 3.4% scaling uncertainty due to the beam polarization measurements is not shown.

$\pi^{\pm}$	p_T range (GeV/c)	A_N (10^{-3})	ΔA_N (10^{-3})	δA_N (10^{-3})
π^-	5–6	6.30	4.67	0.03
	6–7	9.98	4.73	0.95
	7–8	3.71	6.60	0.55
	8–11	0.44	6.85	0.10
	11–15	−9.27	11.76	5.60
π^+	5–6	−5.60	4.33	1.55
	6–7	−0.44	4.49	0.10
	7–8	−6.81	6.12	0.23
	8–11	3.99	5.91	2.70
	11–15	15.43	11.83	6.33

for either pion charge. Higher statistical precision, as is envisioned to be extracted with the sPHENIX experiment [24], will tell whether different flavors produce different asymmetries. It is worth noting that while the knowledge on the higher-twist correlations is still very limited, both the Sivers functions as well as the combinations of quark transversity and Collins fragmentation functions, show clear differences for up- and down-quark related effects.

When comparing the asymmetries to the expected asymmetries based on the global fit of data from SIDIS, other (predominantly forward) single-spin asymmetries in $p + p$ collisions, and e^+e^- data [16], the PHENIX results at higher transverse momenta are well described. In the midrapidity range, these calculations are dominated by the higher twist quark-gluon-quark correlators in the nucleon that are related to the quark Sivers functions. However, at lower transverse momenta, the size and sign of the measured asymmetries, especially for negative pions, appear to be slightly different.

VII. SUMMARY

In summary, the PHENIX experiment has measured charged-pion transverse-single-spin asymmetries at central rapidities. The precision has been greatly improved from the previously published nonidentified charged-hadron asymmetries [25] to a one-percent-level precision of charged pions over a substantially larger range of transverse momenta. While the asymmetries overall are consistent with zero, as well as the previously published neutral-pion asymmetries in the same rapidity region, an indication for a charge-dependent separation of the asymmetries is visible. If confirmed with higher precision, it could indicate a flavor-dependent effect.

[1] D. Adams *et al.* (E581, E704 Collaborations), Comparison of spin asymmetries and cross-sections in π^0 production by 200-GeV polarized antiprotons and protons, Phys. Lett. B **261**, 201 (1991).

[2] L. Adamczyk *et al.* (STAR Collaboration), Transverse single-spin asymmetry and cross section for π^0 and η mesons at large Feynman x in $p^\uparrow + p$ collisions at $\sqrt{s} = 200$ GeV, Phys. Rev. D **86**, 051101 (2012).

[3] A. Adare *et al.* (PHENIX Collaboration), Measurement of transverse-single-spin asymmetries for midrapidity and forward-rapidity production of hadrons in polarized $p + p$ collisions at $\sqrt{s} = 200$ and 62.4 GeV, Phys. Rev. D **90**, 012006 (2014).

[4] U. A. Acharya *et al.* (PHENIX Collaboration), Probing Gluon Spin-Momentum Correlations in Transversely Polarized Protons through Midrapidity Isolated Direct Photons in

$p^\uparrow + p$ Collisions at $\sqrt{s} = 200$ GeV, Phys. Rev. Lett. **127**, 162001 (2021).

[5] G. L. Kane, J. Pumplin, and W. Repko, Transverse Quark Polarization in Large p_T Reactions, e^+e^- Jets, and Leptoproduction: A Test of QCD, Phys. Rev. Lett. **41**, 1689 (1978).

[6] S. Benic, Y. Hatta, H.-N. Li, and D.-J. Yang, Single-spin asymmetries at two loops, Phys. Rev. D **100**, 094027 (2019).

[7] D. W. Sivers, Single-spin production asymmetries from the hard scattering of point-like constituents, Phys. Rev. D **41**, 83 (1990).

[8] J. C. Collins, Fragmentation of transversely polarized quarks probed in transverse-momentum distributions, Nucl. Phys. **B396**, 161 (1993).

[9] A. Airapetian *et al.* (HERMES Collaboration), Single-Spin Asymmetries in Semi-Inclusive Deep-Inelastic Scattering

on a Transversely Polarized Hydrogen Target, Phys. Rev. Lett. **94,** 012002 (2005).

[10] A. Efremov, V. Korotkiian, and O. Teryaev, The twist-three single-spin asymmetries of pion production, Phys. Lett. B **348,** 577 (1995).

[11] J. Qiu and G. Sterman, Single-transverse-spin asymmetries in hadronic pion production, Phys. Rev. D **59,** 014004 (1998).

[12] Y. Kanazawa and Y. Koike, Estimate of a chiral odd contribution to single-transverse-spin asymmetry in hadronic pion production, Phys. Lett. B **490,** 99 (2000).

[13] A. Metz and D. Pitonyak, Fragmentation contribution to the transverse single-spin asymmetry in proton-proton collisions, Phys. Lett. B **723,** 365 (2013); **762,** 549(E) (2016).

[14] A. Bacchetta, D. Boer, M. Diehl, and P. J. Mulders, Matches and mismatches in the descriptions of semi-inclusive processes at low and high transverse momentum, J. High Energy Phys. 08 (2008) 023.

[15] J. P. Ralston and D. E. Soper, Production of dimuons from high-energy polarized proton-proton collisions, Nucl. Phys. **B152,** 109 (1979).

[16] J. Cammarota, L. Gamberg, Z.-B. Kang, J. A. Miller, D. Pitonyak, A. Prokudin, T. C. Rogers, and N. Sato (Jefferson Lab Angular Momentum Collaboration), Origin of single transverse-spin asymmetries in high-energy collisions, Phys. Rev. D **102,** 054002 (2020).

[17] U. A. Acharya *et al.* (PHENIX Collaboration), Transverse-single-spin asymmetries of midrapidity π^0 and η mesons in polarized $p + p$ collisions at $\sqrt{s} = 200$ GeV, Phys. Rev. D **103,** 052009 (2021).

[18] RHIC Polarimetry Group, RHIC polarization for Runs 9–12, RHIC/CAD Accelerator Physics Note, 490 (2018).

[19] K. Adcox *et al.* (PHENIX Collaboration), PHENIX detector overview, Nucl. Instrum. Methods Phys. Res., Sect. A **499,** 469 (2003).

[20] A. Adare *et al.* (PHENIX Collaboration), Inclusive cross section and single-transverse-spin asymmetry for very forward neutron production in polarized $p + p$ collisions at $\sqrt{s} = 200$ GeV, Phys. Rev. D **88,** 032006 (2013).

[21] R. Brun, F. Bruyant, F. Carminati, S. Giani, M. Maire, A. McPherson, G. Patrick, and L. Urban, GEANT detector description and simulation tool, Reports No. CERN-W5013, No. CERN-W-5013, No. W5013, No. W-5013, 1994.

[22] T. Sjöstrand, L. Lönnblad, and S. Mrenna, PYTHIA 6.2: Physics and manual, arXiv:hep-ph/0108264.

[23] A. Adare *et al.* (PHENIX Collaboration), Charged-pion cross sections and double-helicity asymmetries in polarized $p + p$ collisions at $\sqrt{s} = 200$ GeV, Phys. Rev. D **91,** 032001 (2015).

[24] sPHENIX Collaboration, The sPHENIX experiment, https://www.sphenix.bnl.gov/ (2017).

[25] S. S. Adler *et al.* (PHENIX Collaboration), Measurement of Transverse-Single-Spin Asymmetries for Midrapidity Production of Neutral Pions and Charged Hadrons in Polarized $p + p$ Collisions at $\sqrt{s} = 200$ GeV, Phys. Rev. Lett. **95,** 202001 (2005).